Letters

Frequency-Domain Complementary Operators for Finite-Elements Simulation

Omar M. Ramahi

***Abstract*—A new mesh-truncation technique is introduced for the frequency-domain (time-harmonic) solution of open-region radiation problems. The technique is based on the complementary operators method (COM), where two independent solutions are averaged to eliminate first-order boundary reflections. The dual complementariness in the frequency domain is achieved by introducing a discrete-domain operator that achieves the objective of ∂_t in the original time-domain development of COM.**

***Index Terms*—Absorbing boundary conditions, finite-element methods.**

I. Introduction

The complementary operators method (COM) has been successfully used for open-region mesh truncation in the finite-difference time-domain (FDTD) solution of wave propagation problems [1]–[3]. The underlying mechanism of COM is two auxiliary differential operators, ∂_x and ∂_t. These two operators are applied separately on an absorbing boundary condition (ABC) such as Higdon, Liao, etc. The purpose of the auxiliary operators is to produce reflection coefficients that are 180° out of phase, not only in the analytic domain, but also in the discrete domain. By averaging the solutions obtained from the application of each of the two operators on an ABC, a new solution is obtained that is devoid of first-order reflections.

In [1]–[3], the COM theory has been fully developed for time-domain simulation. In the frequency domain, the analogous dual of ∂_t and ∂_x must be obtained. This poses a difficulty. The implementation of ∂_x in the frequency domain is straightforward. However, accomplishing the effect of ∂_t cannot take place by a simple conversion to $j\omega$ since such conversion does not have the desired effect on the numerical implementation. In this work, this difficulty is overcome by introducing a new operator, which is analogous to ∂_t and achieves its objective in the time domain.

II. Frequency-Domain Complementary Operators

We consider the problem of wave propagation in open region (free-space). [The development here is applicable to the two- (2-D) or three-dimensional (3-D) space.] Let us consider a planar outer boundary normal to the x-axis. Let B denote the operation of an ABC. Applying B on the field u, we have

$$Bu = 0. \tag{1}$$

The reflection coefficient that results from the application of B, denoted as $R(B)$, is found by representing the field at the boundary in terms of outgoing and incoming plane waves

$$u = e^{-jk_x x} + R(B)e^{jk_x x}. \tag{2}$$

Manuscript received March 20, 1999; November 22, 1999.

The author is with Compaq Computer Corporation, MRO1-1/p5, Marlborough, MA, 01752-3085 USA (email: Omar.Ramahi@compaq.com).

Publisher Item Identifier S 0018-926X(00)03247-6.

The first of the two complementary operators is constructed by applying ∂_x on B

$$(\partial_x B)u = 0. \tag{3}$$

The reflection coefficient corresponding to $\partial_x B$ can be obtained by applying (3) on (2) to give

$$R(\partial_x B) = -R(B). \tag{4}$$

When implemented numerically, however, the reflection coefficient due to $\partial_x B$ is affected by the discretization of the domain [2]. Therefore, to account for this discretization, we represent the field as

$$u = e^{-jk_x i\Delta x} + Re^{jk_x i\Delta x} \tag{5}$$

where i is the space index in the x-direction. Naturally, the representation of the field, as in (5), assumes structured grid in the boundary region.

Approximating ∂_x in (3) as a backward finite difference, we have

$$\partial_x \approx D_x = \frac{I - S^{-1}}{\Delta x} \tag{6}$$

where I is the identity operator and S^{-1} is the shift operator. Finally, substituting (6) into (4) and applying the resulting operator on (5), we have

$$R(\partial_x B) \approx R(D_x B^d) = (-1)e^{jk_x \Delta x} R(B^d) \tag{7}$$

where B^d denotes the boundary operator B in the discrete domain.

Notice that once in the discrete domain, the division by Δx in (6) becomes inconsequential since the operation of $\partial_x B$ is equated to zero. Therefore, we can use the difference operator $\Delta = I - S^{-1}$ instead of the finite-difference one in (6) to arrive at the same reflection coefficient in (7), viz.

$$R(D_x B^d) \approx R(\Delta B^d) = -e^{jk_x \Delta x} R(B^d). \tag{8}$$

For the complementary operation to be exact, we need a second complementary operator that gives a reflection coefficient of $-R(\Delta B^d)$. This can be accomplished by defining a new discrete-domain operator, which we denote by $\bar{\Delta}$

$$\bar{\Delta} = I + S^{-1}. \tag{9}$$

Applying $\bar{\Delta}$ on B^d, we have

$$R(\bar{\Delta} B^d) = e^{jk_x \Delta x} R(B^d). \tag{10}$$

The reflection coefficients in (8) and (10) are precisely 180° out of phase, thus achieving full complementariness.

III. Numerical Implementation

The complementary operators are applicable only on boundaries that are parallel to the Cartesian coordinates. In this respect, their implementation is similar to perfectly matched layer (PML) truncation techniques. For B in the above equations, we use Higdon's ABC's [4],

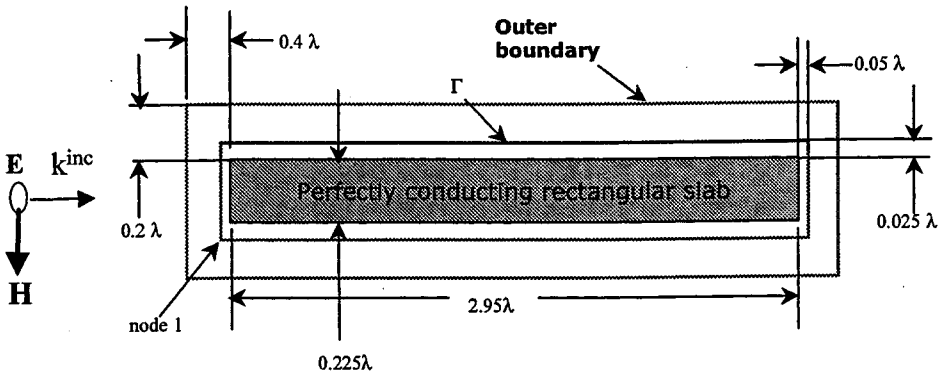

Fig. 1. Computational domain used for the problem of E-polarization scattering by a perfectly conducting rectangular slab.

which were developed for time-domain mesh truncation after carrying out the conversion to the frequency domain.

Higdon's Nth-order operator in the frequency domain is expressed as

$$B = (\partial_n + jk)^N \tag{11}$$

where k is the wave number and $n = x, y, z$. Implementing (11) using backward finite-difference approximation for ∂_n, we have

$$B^d = [(1 + jk\Delta h)I - S^{-1}]^N \tag{12}$$

where $\Delta h = \Delta x, \Delta y, \Delta z$. Therefore, the two complementary operators simply become

$$\Delta B^d = (I - S^{-1})[(1 + jk\Delta h)I - S^{-1}]^N \tag{13}$$

$$\bar{\Delta} B^d = (I + S^{-1})[(1 + jk\Delta h)I - S^{-1}]^N. \tag{14}$$

An important requirement for the implementation of the above operators is an orthogonal grid in the boundary region. The minimum width of this grid depends on the order of the operator employed.

The numerical implementation of the two discrete-domain complementary operators ΔB^d and $\bar{\Delta} B^d$ in a frequency-domain finite-element code is made possible by the recently introduced methodology in [5]. In [5], a procedure was introduced to incorporate Bayliss–Turkel (BT) ABC's of any order in a finite-element code. Since the discrete-domain complementary operators introduced in this work are identical in form to the BT operators, the implementation of COM follows an identical procedure to that in [5].

The effectiveness of this new construction is demonstrated by considering a numerical experiment in 2-D space in which we study the problem of E-polarization scattering by a thin perfectly conducting slab measuring $0.225\lambda \times 2.95\lambda$. The direction of the incident wave is taken to be parallel to the long axis of the slab as shown in Fig. 1. The outer boundary is positioned such that the separation between it and the conductor is 0.4λ from the left- and right-hand sides and 0.2λ from the top and bottom, as illustrated in Fig. 1. Fig. 2 shows the magnitude of the scattered electric field on the observation contour Γ, which is highlighted in Fig. 1. A total of 148 nodes span the observation contour Γ. The numbering of the nodes starts at the lower left-hand corner and proceeds clockwise. Due to the symmetry of the problem, results are only shown for field values on the upper half of the contour. For comparison, the method of moments (MoM) solution is also provided, along with the solutions obtained using Higdon's second- and third-order boundary conditions. The COM solution employed Higdon's third-order ABC ($N = 3$ in (13) and (14)), which, after the application of Δ and $\bar{\Delta}$ results in a fourth-order difference operation. The numerical results presented in Fig. 2 show very strong agreement between the MoM and the COM solutions. Such strong agreement is achieved in spite of the very close proximity of the outer boundary to the conductor.

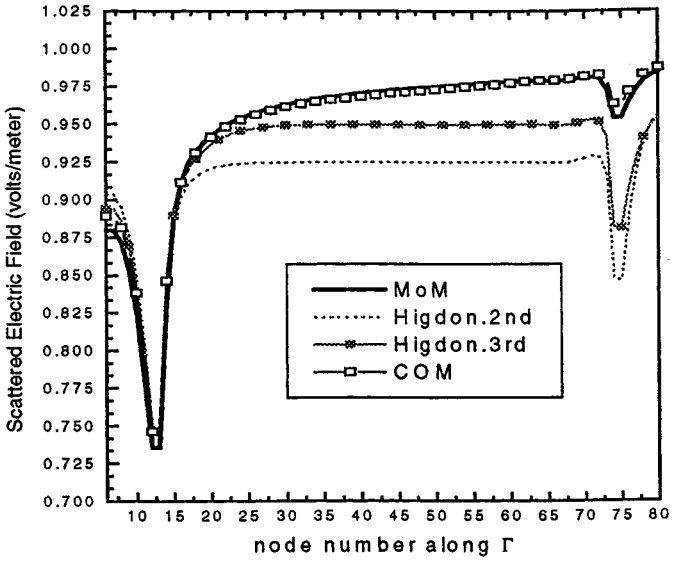

Fig. 2. Scattered electric field calculated on the contour Γ using the MoM and the finite-element method employing the COM, Higdon's second-order ABC (Higdon 2nd), and Higdon's third-order ABC (Higdon 3rd).

IV. Conclusion

This paper presented the development of frequency-domain complementary operators. The complementariness is achieved in both the analytic and discrete domains. A numerical experiment was presented in 2-D space showing the effectiveness and practicality of this new scheme.

The application of this method requires two independent simulations of the problem. Despite this, however, computer memory and execution time can be saved by positioning the outer mesh-truncating boundary very close to the conductor as was demonstrated in the numerical example presented.

REFERENCES

[1] O. M. Ramahi, "Complementary operators: A method to annihilate artificial reflections arising from the truncation of the computational domain in the solution of partial differential equations," *IEEE Trans. Antennas Propagat.*, vol. 43, pp. 697–704, July 1995.

[2] ——, "Complementary boundary operators for wave propagation problems," *J. Computat. Phys.*, vol. 133, pp. 113–128, 1997.

[3] ——, "The concurrent complementary operators method for FDTD mesh truncation," *IEEE Trans. Antennas Propagat.*, vol. 46, pp. 1475–1482, Oct. 1998.

[4] R. L. Higdon, "Radiation boundary conditions for elastic wave propagation," *SIAM J. Numer. Anal.*, vol. 27, no. 4, pp. 831–870, Aug. 1990.

[5] O. M. Ramahi, "Exact implementation of higher-order Bayliss-Turkel absorbing boundary operators in finite element simulation," *IEEE Microwave Guided Wave Lett.*, vol. 8, pp. 360–362, Nov. 1998.

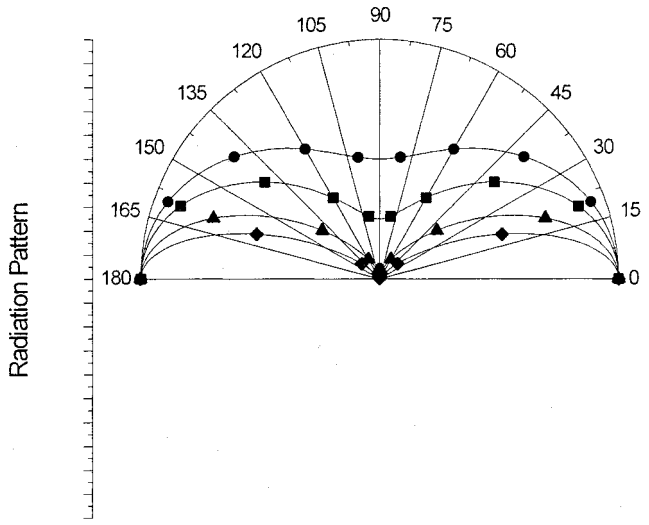

Fig. 1. Radiation pattern sustained by a vertical electric source for different values of $\varepsilon_r^{(1)}$ ($f = 10$ GHz, $d = 1.55$ mm, $h = 1.0$ mm, ■ $\varepsilon_r^{(1)} = 2.1$, • $\varepsilon_r^{(1)} = 2.5$, △ $\varepsilon_r^{(1)} = 3$, ◇ $\varepsilon_r^{(1)} = 4$).

Full-Wave Analysis of Planar Stratified Media with Inhomogeneous Layers

Lucio Vegni and Alessandro Toscano

***Abstract*—In this paper, the dyadic Green's functions for an inhomogeneous isotropic grounded slab embedded in an unbounded isotropic half-space fed by an electric three-dimensional (3-D) point-source based on the equivalent two-port circuit representation along the axis normal to the stratification is presented. The working case is extensively investigated by deriving important information on the radiation of the structure and on how to control the radiation on the horizon plane. Numerical results are also presented showing the effects of the electromagnetic parameters on radiation pattern of the integrated structure.**

***Index Terms*—Green's dyad, inhomogeneous media, layered media, spectral domain.**

I. INTRODUCTION

In the past few years, the attention paid to the study of electromagnetic propagation in inhomogeneous media has increased notably. This increasing interest is raised by the potential applications of the inhomogeneous material as well as its theoretical and academic significance.

The most outstanding properties of inhomogeneous media concerning the propagation of electromagnetic fields are reported to be their ability either for enlarging the bandwidth and for improving the coupling effects due to the surface waves.

Although today there are no known natural media showing inhomogeneity properties at microwave and millimeter frequencies, the progress in the polymers science is expected to make these media of common use in future technology. In this event, many of the proposed devices whose performance lies on the inhomogeneity properties of the media could be built.

The electromagnetic propagation in inhomogeneous materials has not been extensively studied in the literature. General features on the bi(iso/ani)sotropic materials are presented in [1] and different aspects about electromagnetic propagation in homogeneous stratified bi(iso/ani)sotropic media are considered in [2]. Propagation along closed waveguides inhomogeneously filled with isotropic materials has been considered for example in [3]. A microstrip on an homogeneous stratified substrate is analyzed in [4].

Since, to the authors' knowledge, no method has been reported to compute in a closed analytical form the complete electric and magnetic spectral Green's dyad for layered media with inhomogeneous layers, in this paper the Green's functions for such media will be presented.

Finally, numerical results will be shown to see the effect of the inhomogeneity on the electromagnetic behavior of the stratified structure.

Manuscript February 19, 1999; January 15, 1999.

The authors are with the Department of Electronic Engineering, Third University of Rome, Rome, I-00146 Italy.

Publisher Item Identifier S 0018-926X(00)03244-0.

II. ANALYTICAL DEVELOPMENT

Let us now consider an isotropic inhomogeneous medium characterized by a dielectric constant $\varepsilon(y)$ and a magnetic permeability $\mu(y) = 1$.

Following the method developed in [6] for the bianisotropic homogeneous case, we start from the Maxwell's equations in presence of electric $\mathbf{J}$ and magnetic $\mathbf{M}$ sources ($e^{j\omega t}$ is assumed).

By applying the two-dimensional (2-D) Fourier transform defined as in [5] and by rotating the Cartesian coordinate system $\Omega(x, y, z)$ into the associated one $\Omega(v, y, u)$ defined by the matrix $\underline{\mathbf{T}}$ [5] with:

$$\begin{cases} \alpha = \xi \sin(\delta) \\ \beta = \xi \cos(\delta) \end{cases}$$

under the following hypotheses on the constitutive relations: 1) $\varepsilon(y) = (\varepsilon_r^{(1)}/y)$; 2) $\varepsilon(y) = (\varepsilon_r^{(2)}/y^2)$; and 3) $\varepsilon(y) = \varepsilon_r e^{-Ky}$ it is possible to show that the analytical solutions for the spectral electromagnetic field components $\tilde{E}_u$ and $\tilde{H}_u$ in the three cases are:

1) when $\varepsilon(y) = (\varepsilon_r^{(1)}/y)$ for $y \neq 0$:

$$\begin{cases} \tilde{E}_u = \dfrac{e^{-y\xi}}{y}\left[C_1 M\left(\dfrac{\xi - k_0^2\varepsilon_r^{(1)}}{2\xi}, 2, 2y\xi\right) + C_2 U\left(\dfrac{\xi - k_0^2\varepsilon_r^{(1)}}{2\xi}, 2, 2y\xi\right)\right] \\ \tilde{H}_u = e^{-y\xi}\left[D_1 M\left(\dfrac{\xi - k_0^2\varepsilon_r^{(1)}}{2\xi}, 1, 2y\xi\right) + D_2 U\left(\dfrac{\xi - d_{\mathrm{TE}}}{2\xi}, 1, 2y\xi\right)\right] \end{cases} \tag{1}$$

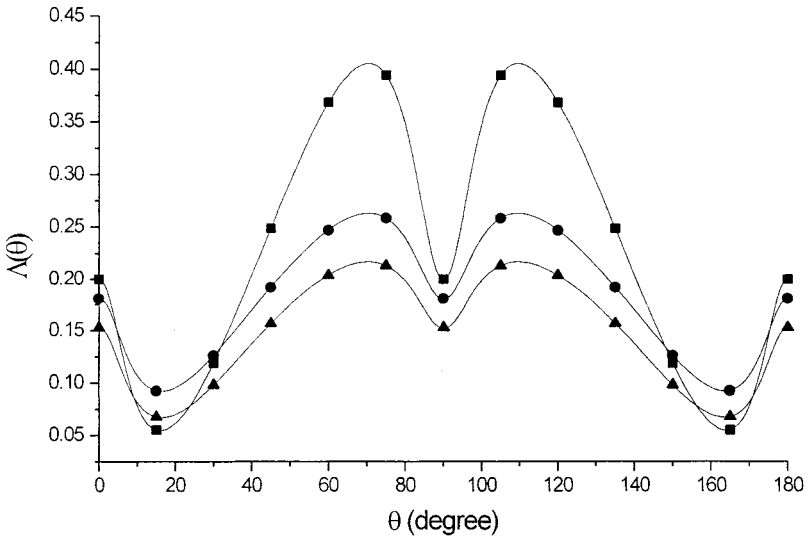

Fig. 2. Examples of radiation on the horizon plane ($f = 10$ GHz, ■ $d = 12$ mm, $h = 4$ mm, $\varepsilon_r^{(2)} = 1$, • $d = 8.7$ mm, $h = 2.9$ mm, $\varepsilon_r^{(2)} = 3$, △ $d = 15$ mm, $h = 5$ mm, $\varepsilon_r^{(2)} = 5.2$).

2) when $\varepsilon(y) = (\varepsilon_r^{(2)}/y^2)$, for $y \neq 0$:

$$\begin{cases} \tilde{E}_u = \sqrt{y}\left[C_1 \,\mathrm{Bessel}\, I\left(-\frac{1}{2}\sqrt{1-4k_0^2\varepsilon_r^{(2)}}, y\xi\right)\right. \\ \qquad \left. + C_2 \,\mathrm{Bessel}\, I\left(\frac{1}{2}\sqrt{1-4k_0^2\varepsilon_r^{(2)}}, y\xi\right)\right] \\ \tilde{H}_u = \frac{1}{\sqrt{y}}\left[D_1 \,\mathrm{Bessel}\, I\left(-\frac{1}{2}\sqrt{1-4k_0^2\varepsilon_r^{(2)}}, y\xi\right)\right. \\ \qquad \left. + D_2 \,\mathrm{Bessel}\, I\left(\frac{1}{2}\sqrt{1-4k_0^2\varepsilon_r^{(2)}}, y\xi\right)\right] \end{cases} \tag{2}$$

3) when $\varepsilon(y) = \varepsilon_r e^{-Ky}$, letting $\rho = \sqrt{K^2+4\xi^2}/K, \sigma = 2(k_0/K)\sqrt{\varepsilon_r}$:

$$\begin{cases} \tilde{E}_u = C_1 \,\mathrm{Bessel}\, J\left(-\frac{2\xi}{K}, \sigma e^{-\frac{Ky}{2}}\right) \\ \qquad + C_2 \,\mathrm{Bessel}\, J\left(\frac{2\xi}{K}, \sigma e^{-\frac{Ky}{2}}\right) \\ \tilde{H}_u = \frac{e^{-K\frac{y}{2}}}{\xi}\left[D_1 \,\mathrm{Bessel}\, J\left(-\rho, \sigma e^{-\frac{Ky}{2}}\right)\right. \\ \qquad \left. + D_2 \,\mathrm{Bessel}\, J\left(\rho, \sigma e^{-\frac{Ky}{2}}\right)\right] \end{cases} \tag{3}$$

$M(a,b,c)$ and $U(a,b,c)$ are the hypergeometric confluent functions, $\mathrm{Bessel}\, J[n,z]$ gives the Bessel function of the first kind: $J_n(z)$. $\mathrm{Bessel}\, I[n,z]$ gives the modified Bessel function of the first kind $I_n(z)$.

The elements of the first and third row of the spectral electric Green's dyad may be obtained in terms of the integrals of the wave equations for $\tilde{E}_u$ in the grounded slab and in the isotropic half-space, respectively, by making use of the equivalent transmission line representation of the material which fills the grounded slab as a superposition of $\mathbf{TE}(\hat{\mathbf{y}})$ and $\mathbf{TM}(\hat{\mathbf{y}})$ spectral waves [5]. The elements $\tilde{G}_{xy}$ and $\tilde{G}_{zy}$ can be derived by applying the reciprocity theorem together with the Parsevaal theorem [5]. From the transmission line equations and the discontinuity relations proper of the point-source excitation the $\tilde{G}_{yy}$ term for each one of the three regions into which the structure is divided can be obtained in a very straightforward manner [5].

III. Numerical Results

In order to present an example of determination of the radiated electromagnetic field by applying the spectral theory we consider the case of a three-dimensional (3-D) electric point-source embedded in an homogeneous isotropic grounded slab at the $y = -h$ plane.

The spatial electromagnetic field radiated in a spherical coordinate system $\Omega(r,\theta,\varphi)$ can be evaluated by applying the equivalence theorem in the interface plane $y = 0$. In this section, some examples of radiated patterns are shown for different values of the electromagnetic parameters under both vertical and planar excitation conditions. The role of the inhomogeneity can be fully examined by comparison with the homogeneous case as shown in Fig. 1 for an inhomogeneous isotropic grounded slab characterized by different dielectric constant profiles. From this figure it is observed that the inhomogeneous material exhibits an increased directivity in the radiation pattern. As it is well evident, the behaviors of the radiation patterns are strongly affected by $\varepsilon(y)$. Therefore, the inhomogeneity controls in a strong way the value and the directivity of the radiated pattern. Fig. 1 also gives some information about the reduction of the radiation in the $\varphi = 0^\circ, 90^\circ$ planes. This means that in far zone the effect of the electromagnetic waves traveling with wave numbers parallel to the x-y plane becomes negligible. This result may lead to an increased radiation efficiency of the structure when inhomogeneous grounded slabs with metallic patches are used as printed antennas.

Finally, in Fig. 2 we show the effect of the inhomogeneity on the radiation along the $\hat{\mathbf{z}}$-axis of the horizon plane. For some practical applications (for instance: microstrip patch antennas in array configuration) it is important to know and control the radiation on the horizon plane.

References

[1] B. S. Agrawal and E. Bahar, "Propagation of electromagnetic waves in inhomogenous anisotropic media," *IEEE Trans. Antennas Propagat.*, vol. AP-28, pp. 422–424, Apr. 1980.

[2] J. R. Mosig and T. K. Sarkar, "Comparison of quasi-static and exact electromagnetic fields from an horizontal electric dipole above a lossy dielectric backed by an imperfect ground plane," *IEEE. Trans. Microwave Theory Tech.*, vol. MTT-34, pp. 379–387, Apr. 1986.

[3] W. Schlosser and H. G. Unger, "Partially filled waveguides and surface waveguides of rectangular cross-section," in *Advances in Microwaves*. New York: Academic, 1986.

[4] K. A. Michalski and D. Zheng, "Electromagnetic scattering and radiation by surfaces of arbitrary shape in layered media—Part II: Implementation and results for contiguous half-spaces," *IEEE Trans. Antennas Propagat.*, vol. 38, pp. 345–352, Mar. 1990.

[5] L. Vegni, R. Cicchetti, and P. Capece, "Spectral dyadic Green's function formulation for planar integrated structures," *IEEE Trans. Antennas Propagat.*, vol. 36, pp. 1057–1065, Aug. 1998.
[6] A. Toscano and L. Vegni, "Electromagnetic waves in planar integrated pseudochiral Ω structures," *Progress Electromagn. Res.—Special Issue Bianisotropic Bi-Isotropic Media Applicat.*, vol. 9, pp. 181–216, Dec. 1994.
[7] B. Popovski, A. Toscano, and L. Vegni, "Radial and asymptotic closed form representation of the spatial microstrip dyadic Green's function," *J. Electromagn. Waves Applicat.*, vol. 9, pp. 97–126, Jan. 1995.

Phased-Array Radiator Reflection Coefficient Extraction from Computer Waveguide Simulator Data When Grating Lobes Are Present

Eric L. Holzman

***Abstract*—Commercially available finite-element software that solves Maxwell's equations for arbitrary three-dimensional bounded structures has enabled phase-array radiator designers to perform waveguide simulator modeling of phased-array radiating elements on the computer very efficiently. Published work on waveguide simulator design has concentrated on array performance in the absence of grating lobes, a requirement for many radar applications. For such simulators, the reflection coefficient of each propagating mode at the waveguide simulator port gives the radiator reflection coefficient at a discrete scan angle. However, the design of limited scan arrays can lead to selection of an array element spacing that allows grating lobes in real space. When a waveguide simulator is modeled on the computer, and a grating lobe is present, the two waveguide modes representing the main lobe and the grating lobe will propagate in the waveguide simulator and they will be coupled together. The simulator port-reflection coefficient of either mode is not the true reflection coefficient seen by the radiating element. We describe a method for extracting the reflection coefficient of the radiating element from the waveguide simulator data when one or more grating lobes are present.**

***Index Terms*—Grating lobes, phased-array antennas, reflection coefficient.**

I. Introduction

The use of waveguide simulators to determine the reflection coefficient of phased-array radiating elements in an infinite array environment is widespread. The development of fast user-friendly commercially available finite-element software in the 1990's has made possible waveguide simulator modeling of phased-array radiating elements on the computer. Eisenhart [1] provides an excellent discussion including detailed examples of the computerized method and its many advantages. His discussion and other published work on waveguide simulator design theory (see references in [1]) focus on array performance in the absence of grating lobes, a requirement for many radar applications. However, the design of limited scan arrays can lead to the selection of an array element spacing that allows grating lobes in real space. For example, a phased array placed in geosynchronous orbit might have a relatively wide element separation, two wavelengths or more, to minimize the number of elements. The array can point its main beam anywhere on the Earth's surface within a scan cone of 20° and keep its grating lobes pointed into empty space. When a waveguide simulator is modeled on the computer and a grating lobe is present, extraction of the radiator reflection coefficient from the S-parameter data is not completely straightforward. In this paper, we present a method for extracting the reflection coefficient of the radiating element from the waveguide simulator data.

The author was with Lockheed Martin GES, Moorestown, NJ 08057. He is now with Telaxis Communications Corporation, South Deerfield, MA 01373 USA.

Publisher Item Identifier S 0018-926X(00)03248-8.

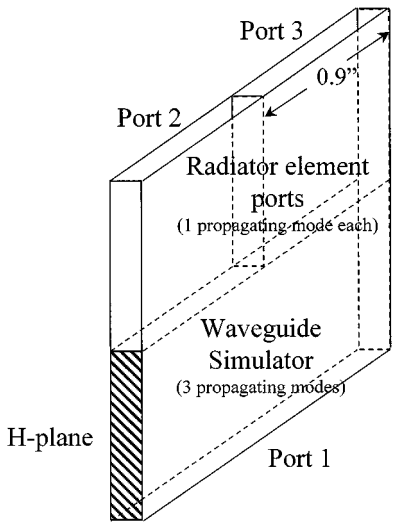

Fig. 1. Two radiator cell waveguide simulator. TE_{10} mode propagates in each waveguide radiator. Radiators are separated by zero-thickness metal septum. Frequency: 10 GHz.

II. Discussion

Fig. 1 shows a simple waveguide simulator. There are three physical ports to this simulator. At the top of the figure are two waveguide radiating elements (ports 2 and 3), which, in an actual array, would be connected to phase shifters or T/R modules and an RF beamformer. Each of the waveguide radiator cells propagates a single TE_{10} mode (not to be confused with the simulator modes). For this example, the element spacing and frequency have been chosen so that a grating lobe will appear when the beam is scanned past 18°. At the bottom of the figure, the waveguide simulator propagates three modes. Note that one narrow wall of the simulator is a perfect magnetic conductor and the other is a perfect electric conductor (creating a compact structure equivalent to a four-cell all-metal simulator). Fundamentally, the reflection coefficient of each propagating mode at the waveguide simulator port gives the radiator reflection coefficient at a discrete scan angle, which is a function of the frequency of analysis, the mode's field configuration, and the cutoff frequency. In our example, the three modes correspond to three pairs of H-plane scan angles, $\pm 9.43°$, $\pm 29.46°$, and $\pm 55.05°$. Table I shows the S-parameter data, simulator mode propagation coefficients and corresponding scan angles obtained from the computer model. When a grating lobe is not present in real space, we can interpret the S-parameter data obtained from a computer waveguide simulator in a straightforward manner. For a scan angle of 9.4°, the magnitude of S_{11}, mode 1 is the phased-array radiator reflection coefficient in the infinite array environment. Any energy reflected at the radiator/simulator interface reflects back in mode 1 only.

In contrast to mode 1, simulator modes 2 and 3 are coupled together. As Eisenhart shows in [1], the existence of a grating lobe is the cause. When the array is scanned to $+29.46°$ (simulator mode 2), a grating lobe will appear at $-55.05°$ (simulator mode 3). Conversely, when the

TABLE I
SCATTERING PARAMETER MATRIX, MODE PROPAGATION CONSTANTS AND SIMULATOR SCAN ANGLES. PORT 1 IS WAVEGUIDE SIMULATOR, AND PORTS 2 AND 3 ARE RADIATING ELEMENT PORTS. FREQUENCY: 10 GHz. HIGHLIGHTED PARAMETERS ARE COUPLED SIMULATOR MODES 2 and 3

S-MATRIX	Port 1, mode 1	Port 1, mode 2	Port 1, mode 3	Port 2, mode 4	Port 2, mode 5
Port 1, mode 1	0.1343, -44.1°	0.0007, -76.2°	0.0012, 158.9°	0.9155, -60.9°	0.3792, -61.0°
Port 1, mode 2	0.0007, -76.2°	0.3454, 62.1°	0.4689, -39.4°	0.3115, -38.8°	0.7508, 141.2°
Port 1, mode 3	0.0012, 158.9°	0.4689, -39.4°	0.6641,-140.8°	0.2222, 40.0°	0.5383,-140.2°
Port 2, mode 4	0.9155, -60.9°	0.3115, -38.8°	0.2222, 40.0°	0.1154, 101.5°	0.0460, 106.1°
Port 3, mode 5	0.3792, -61.0°	0.7508, 141.2°	0.5383,-140.2°	0.0460, 106.1°	0.0242, 85.0°
Propagat Constant	206.7493 m^{-1}	182.4887 m^{-1}	120.0658 m^{-1}	158.2383 m^{-1}	158.2383 m^{-1}
Scan Angle	9.43°	29.46°	55.05°		

array is scanned to $+55.05^\circ$, a grating lobe appears at -29.46°. From the symmetry of this behavior, we can conclude that the radiator reflection coefficient must be the same for either scan angle, a fact that appears to be contradicted by the highlighted data in Table I. Hence, the simulator port reflection coefficient of either mode cannot be the true reflection coefficient seen by the radiating element.

III. EXTRACTION METHOD

To determine the radiator reflection coefficient, we refer to Fig. 2, which shows a five-port network model of the waveguide simulator in Fig. 1. Each port of the model represents one of the propagating modes, one in each radiator and three in the waveguide simulator. The circled numbers identify the physical ports of the simulator. As Eisenhart states in [1], we can determine the radiator reflection coefficient from either the simulator port (looking in) or the radiating element port (looking out). When a grating lobe is not present, this task is easiest from the simulator side. However, when a grating lobe is present, we must resort to looking out from the radiator side. Because the array is infinite and all radiating elements are identical, the radiator reflection coefficient should be the same in either radiating element port, as our analysis will show. In Fig. 2, Γ_4 and Γ_5 are the unknown radiator reflection coefficients we seek. In terms of the five-port S-parameters, we can write

$$b_4 = S_{41}a_1 + S_{42}a_2 + S_{43}a_3 + S_{44}a_4 + S_{45}a_5$$
$$b_5 = S_{51}a_1 + S_{52}a_2 + S_{53}a_3 + S_{54}a_4 + S_{55}a_5.$$

Now consider that the array is transmitting only. Then, $a_1 = a_2 = a_3 = 0$ because no energy is being received from the simulator port. The above equations simplify considerably

$$b_4 = S_{44}a_4 + S_{45}a_5$$
$$b_5 = S_{54}a_4 + S_{55}a_5.$$

When we solve for the reflection coefficients of the radiating elements, we get

$$\Gamma_4 = b_4/a_4 = S_{44} + S_{45}a_5/a_4 \tag{1}$$

$$\Gamma_5 = b_5/a_5 = S_{54}a_4/a_5 + S_{55}. \tag{2}$$

The ratio a_4/a_5 is an unknown. However, we only want to transmit the two coupled modes represented by b_2 and b_3. Thus, we set b_1 equal to zero, which gives

$$b_1 = S_{14}a_4 + S_{15}a_5 = 0.$$

We solve this equation for the unknown ratio to get

$$a_4/a_5 = -S_{15}/S_{14}. \tag{3}$$

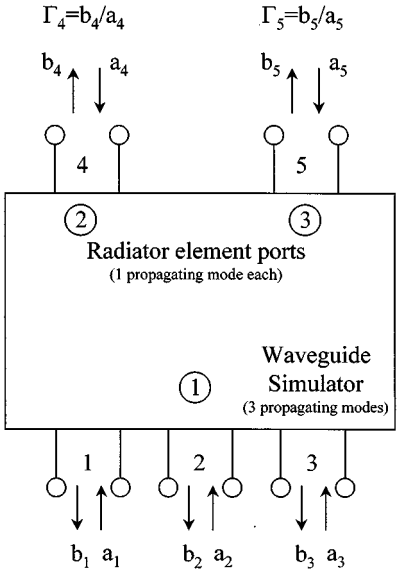

Fig. 2. Five-port network representation of two radiator cell, waveguide simulator. Each port represents a propagating mode. Circled numbers denote physical ports. Γ_4 and Γ_5 are unknown feed coefficients.

Equations (1) and (2) with (3) give the radiating element reflection coefficients

$$\Gamma_4 = S_{44} - S_{45}S_{14}/S_{15} \tag{4}$$

$$\Gamma_5 = -S_{54}S_{15}/S_{14} + S_{55}. \tag{5}$$

If we substitute the values from Table I into these equations, we get $\Gamma_4 = 0.0101, 39.3^\circ$ and $\Gamma_5 = 0.0094, 38.1^\circ$, which are identical within the accuracy of the S-parameter data we used.

We have verified this method against published waveguide array data in which a grating lobe was present [2] and obtained excellent agreement. The same method can be applied to simulators with more radiator cells; the computations just become more tedious and should be done with a computer.

Designers of limited-scan arrays sometimes use highly directive radiators to suppress grating lobes. Even so, our formulation is general and still valid; however, in this case it is unnecessary. If the level of suppression is high, the coupling between the waveguide simulator modes corresponding to the main beam and grating lobes will approach zero and the magnitude of the reflection coefficient at the grating lobe angle will approach unity. Consequently, we can use the conventional procedure of calculating the reflection coefficient from the waveguide simulator port with reasonable accuracy.

IV. Conclusion

We have described a method for extracting the reflection coefficient of a radiating element from waveguide simulator data when one or more grating lobes are present. Because the waveguide simulator modes corresponding to the main beam and grating lobe become coupled, we must determine the radiating element reflection coefficient from the radiating element port, rather than from the waveguide simulator port. However, the reflection coefficient of each radiating element contains contributions from all the waveguide simulator modes. Viewed differently, if we excite the radiating element port mode, all three propagating modes in the simulator port are excited (see data in Table I); thus, the radiating element port reflection coefficients are not meaningful without manipulation. To excite a pair of modes corresponding to a main beam and grating lobe (the example presented in this paper), we must adjust the radiating element excitations to suppress the undesired modes. This procedure is analogous to setting phase shifters in an actual phased array to produce a desired progressive phase distribution across the array.

References

[1] R. L. Eisenhart, "Antenna element and array simulation with commercial software," in *Finite Element Software for Microwave Engineering*, T. Itoh, G. Pelosi, and P. Silvester, Eds. New York: Wiley, 1996.

[2] G. F. Farrel and D. H. Kuhn, "Mutual coupling in infinite planar arrays of rectangular waveguide horns," *IEEE Trans. Antennas Propagat.*, vol. AP-16, pp. 405–414, July 1968.